SPECIAL ISSUES -PROGRESS IN STRUCTURE ANALYSES OF POLYMERIC MATERIALS
BY SYNCHROTRON RADIATION AND NEUTRON BEAM-

Elastic Modulus of the Crystalline Regions of Poly (*p*-phenylene terephthalamide) Single Fiber Using SPring-8 Synchrotron Radiation

Masaru KOTERA,[†] Aya NAKAI, Masahiko SAITO, Takayuki IZU, and Takashi NISHINO

Department of Chemical Science and Engineering, Graduate School of Engineering, Kobe University,
Rokko, Nada, Kobe 657-8501, Japan

ABSTRACT: The elastic modulus, E_l, of the crystalline regions of poly (*p*-phenylene terephthalamide) (PPTA) single fiber in the direction parallel to the chain axis was measured by X-ray diffraction using synchrotron radiation at beamline BL46XU of SPring-8. The E_l value of the PPTA single fiber was obtained as 156 GPa at room temperature from the initial slope of the stress–strain curve of the crystal lattice. However, the inclination of the stress–strain curve changed at a tensile stress of around 1000 MPa, which produced an E_l' value of 199 GPa in a higher stress region. This indicates that the deformation mechanism in the crystal lattice at higher tensile stress was different from that in the initial stage of the tensile deformation. Stress hardening of PPTA was also observed macroscopically during the tensile deformation process. Stress hardening in the crystal lattice was found to directly affect macroscopic stress hardening of the PPTA fiber.   [doi:10.1295/polymj.PJ2007074]
    KEY WORDS   Poly (*p*-phenylene terephthalamide) / Elastic Modulus / Single Fiber / Stress
        Hardening / SPring-8 /

Poly (*p*-phenylene terephthalamide) (PPTA) fiber is one of the most popular high performance polymer fibers. Well known by its commercial names, Kevlar®, and Twaron®, it has excellent thermal stability and good mechanical properties. PPTA fiber is widely used in industrial materials, reinforcement fibers for advanced composite materials, and so on.[1,2] The mechanical properties of PPTA fiber are affected by the microstructures formed during liquid-crystalline spinning. In the last few decades, the relationship between the microstructures and the mechanical properties of PPTA fibers has been extensively studied. Black reported that a possible explanation for the extraordinary mechanical properties of PPTA fiber is its extended chain orientation rather than its high crystallinity.[3] PPTA fiber is said to possess microscopically radially oriented pleated sheet structures, in which the micro-fibrils are misoriented with a long (300–500 nm) zigzag structure along the fiber axis.[4–6] Northolt *et al.* reported that the macroscopic deformation of PPTA fiber is governed by the orientational change in the PPTA micro-fibrils along the fiber axis in the initial tensile stress region.[7,8] Therefore, after the micro-fibril orientation has been completed, stress hardening due to the elongation of the molecular chains themselves is observed in the high tensile stress region. The structural changes during the fiber tensile deformation

process have also been investigated in several studies using a variety of methods, such as Raman spectroscopy,[9–11] an X-ray diffraction method,[7,8,12–21] and a combined microfocus Raman/microfocus X-ray diffraction technique.[22]

The elastic modulus, E_l, of the crystalline regions of polymers in the direction parallel to the chain axis provides important information on the molecular conformation, its deformation process, and its relations to mechanical properties. The E_l value also plays an important role in attempts to obtain high modulus polymer materials because the E_l value is equal to the maximum attainable specimen modulus of a polymer. We measured the E_l value for a variety of polymers using the X-ray diffraction method.[23–26]

X-Ray diffraction has the advantage of selective detection of the crystalline regions. To determine the E_l value experimentally, polymer fibers are constantly stressed and the lattice strains are precisely detected by monitoring the peak shift in the meridional reflection. We have been obtained the E_l value for PPTA fiber as 156 GPa at room temperature.[12–14] For the X-ray diffraction method using a conventional X-ray generator including rotating anode type equipment, a bundle of polymer fiber was used to get sufficient diffraction intensity, because synthetic polymers are known to show weaker diffraction signals. However,

---

there is the worry of stress inhomogeneous distribution within the fiber bundle, and the misalignment of the each fiber may seriously affect the observed E_l value. In addition, the stress–strain curve for PPTA crystalline regions indicated that stress hardening occurred in higher stress region in the E_l measurement, however, whose details are not fully examined. This is because the fiber bundle was used for X-ray diffraction experiments, so the stress applied to the bundle was limited. In contrast, high brilliant synchrotron radiation is expected to produce enough diffraction intensity even from a polymer single fiber. Thus, higher stress could be applied to the single fiber compared with the fiber bundle. Chu *et al.* detected the lattice deformation of PPTA single fiber under tensile stress using a synchrotron wide-angle X-ray diffraction method.[18–20] However, they reported only equatorial 200 and 110 reflection shifts, which correspond to the lattice deformation in the direction perpendicular to the chain axis and tensile stress. Davies *et al.* measured the lattice deformation from meridional layer lines of PPTA single fiber using a microfocus X-ray diffraction technique.[22] In their experiments, the X-ray beam was irradiated in the direction perpendicular to the fiber axis. This geometry was not adequate to detect the meridional Bragg's reflection, and their lattice strain correspondence to that inclined 13.2 degree to the tensile stress. Thus, to evaluate the mechanical properties in the direction exactly parallel to the fiber axis, the lattice deformation of meridional reflections should be used to measure E_l.

In this study, the mechanical deformation of PPTA crystal lattice along the fiber axis was measured using a single fiber by the synchrotron X-ray diffraction method. The structural change in the crystalline regions of PPTA was reported under a high tensile stress of up to 3000 MPa, and its relation to the macroscopic change was investigated.

EXPERIMENTAL

PPTA fiber was supplied by Toray-Du Pont. Co., Ltd. as Kevlar 49®.

The specimen density measured using a floatation method (benzene–carbon tetrachloride system) at 30 °C was obtained as 1.453 g/cm³. The PPTA fiber was observed by a scanning electron microscope (SEM) (HITACHI S-2500) operating at 20 KV.

Synchrotron X-ray diffraction was measured at SPring-8 BL46XU (R&D beamline). X-Ray wavelength is 0.08266 nm (beam size 0.07 mm (horizontal) × 0.5 mm (vertical)).

Figure 1 shows the X-ray fiber photograph of the unloaded PPTA single fiber recorded on a flat-type imaging plate (IP). The sample was exposed to X-
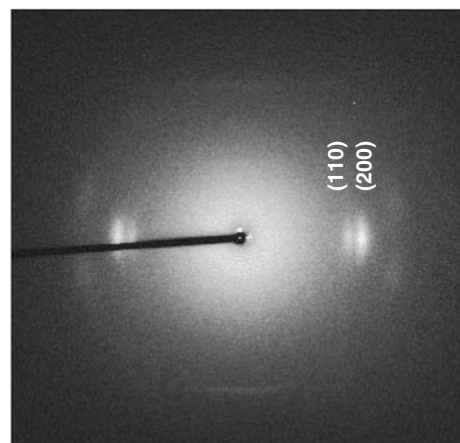

Figure 1. X-ray fiber photograph of PPTA single fiber.

ray for 300 s. The sample to detector distance was 224.5 mm. The SPring-8 synchrotron radiation enabled to give enough diffraction intensity even from a single fiber. Two crystal modifications were reported for PPTA. Among them, all the reflections in this study could be assigned with the monoclinic unit cell: lattice parameter of a = 7.87 Å, b = 5.18 Å, c (fiber axis) = 12.9 Å, and γ = 90 deg.[27] Two strong reflections that were observed on the equator can be indexed as 110 and 200, respectively. These spot-like reflections implied a high degree of crystallite orientation along the fiber axis and a good lateral packing of PPTA molecules in the crystal lattice. The equatorial 200 reflection is often used to evaluate the crystallite orientation of the PPTA fiber.[17,20,28] In order to investigate the change in the crystallite orientation by the applied stress, the full width at half maximum (F_w) value for the 200 reflection along the Debye-Scherrer ring of the PPTA single fiber, detected with IP, was measured under the load. The lower value of the F_w value corresponds to the higher crystallite orientation along the fiber axis.

Figure 2(a) shows the photograph of the stretching device with *X-Y-Z* positioning stages specially designed for the tensile measurement of polymer single fiber. PPTA single fiber (initial length 35 mm) was mounted on a paper window cardholder using an epoxy resin. The paper cardholder was clamped to a stretching device and then cut. The fiber was loaded by symmetric stretching, ensuring that the incident X-ray beam was irradiated on the same position along the fiber during the tensile deformation. This stretching device was set on the center of the goniometer in the SPring-8 BL46XU, as shown in Figure 2(b). The single fiber on the X-ray beam center was aligned using the microscope with a CCD camera, within a *ca.* 30 μm spatial resolution. In order to detect the meridional reflection with a scintillation counter under a constant stress after the stress relaxation (less than
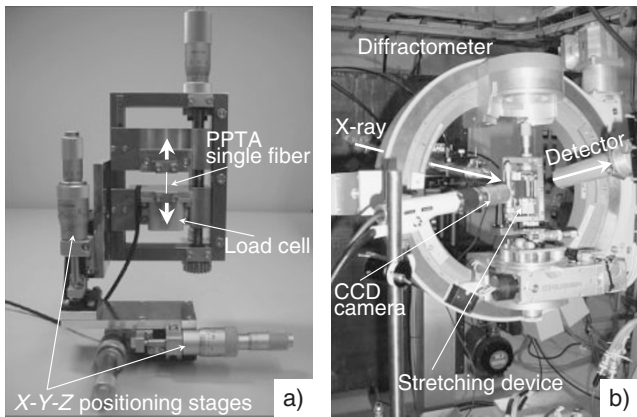
Figure 2. Photographs of (a) the stretching device specially designed for the tensile measurement of polymer single fiber, (b) the X-ray diffractometer in SPring-8 BL46XU (R&D beamline).

3%) was almost completed, a θ-2θ scan was carried out using a symmetric transmission geometry. The strain, ε, of the crystal lattice was calculated by the following equation,

$$\varepsilon = \Delta d / d_0 \qquad (1)$$

where, d_0 is the initial lattice spacing for the meridional 006 reflection determined by Bragg's equation and Δd is the change in the lattice spacing due to the constant tensile stress. The experimental error in measuring the peak shift was evaluated to be less than $\pm 1/100$ degree in diffraction angle of 2θ, which corresponds to a lattice extension of $\pm 0.045\%$. The cross-sectional area of the single fiber was measuring using gravimetric method. The stress on the single fiber was evaluated from the load and the cross-sectional area. The stress σ on the crystalline regions was assumed to be equal to the stress applied to the single fiber. The validity of this assumption of homogeneous stress distribution has been proven for various polymers in earlier studies in that the specimens possess a high degree of crystallinity with high molecular orientation.[23–26] The same E_l value were found for PPTA, Kevlar, Kevlar 29, Kevlar 49, and Kevlar 149 even though the macroscopic modulus changed from 40 GPa to 149 GPa.[11,17,29] Therefore, this assumption is also valid for the series of PPTA fibers. The E_l value was calculated by the following equation;

$$E_l = \sigma / \varepsilon \qquad (2)$$

The macroscopic stress–strain curve of the PPTA single fiber was measured using a tensile tester (Shimadzu, AUTOGRAPH SD-100) at room temperature. The original length of the specimen was 150 mm and the tensile speed was 5 mm/min. In this study, nominal stress and nominal strain was used for calculation.
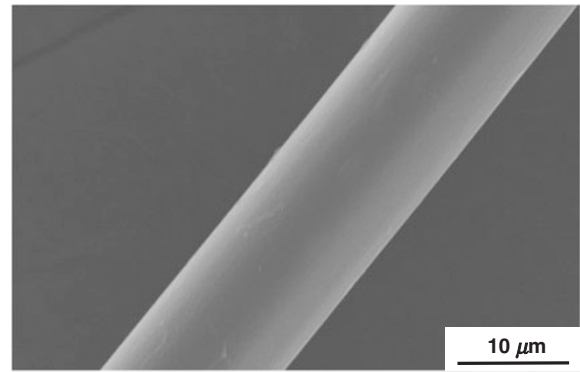

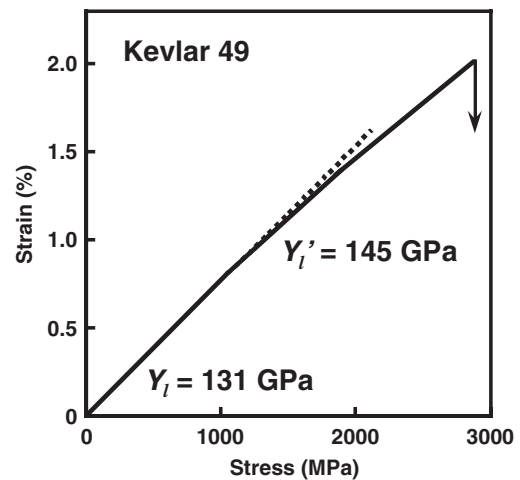**Figure 3.** Scanning electron micrograph of PPTA single fiber.

Figure 4. Macroscopic stress–strain curve for PPTA single fiber.

RESULTS AND DISSCUSSION

Figure 3 shows the SEM photograph of the PPTA single fiber. The fiber surface is very smooth. Its diameter was evaluated as $12.4 \pm 0.3\,\mu m$ by being calibrated using monodispersed polystyrene particle of $2.14\,\mu m$ in diameter. This diameter is equal to that determined by the gravimetric method.

Figure 4 shows the macroscopic stress–strain curve for the PPTA single fiber. The tensile stress increased almost linearly with increasing the strain until the stress reached 1100 MPa. The initial inclination of this curve gave the specimen modulus Y_l of 131 GPa. In contrast, in the higher stress region ($> 1100\,\mathrm{MPa}$), the curve strayed slightly off the initial inclination, and the inclination of the latter half of the curve became larger than that of the initial stage. Here, we defined the inclination of the latter half of the curve as apparent specimen modulus Y_l', and the value of 145 GPa was obtained. This value was calculated using the nominal stress. When this value is re-calculated with consideration the change of cross–sectional area assuming Poisson's ratio of 0.3, using true stress,
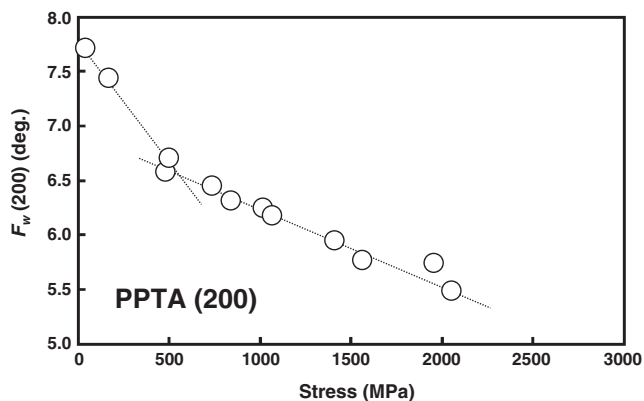
Figure 5. Stress dependence of the F_w value for the 200 reflection of the PPTA single fiber along the azimuthal angle.

Figure 6. Meridional diffraction profiles of the (006) plane of PPTA before loading and under loading (1390 MPa, 2270 MPa).

Y_l of 131.0 GPa change into 131.6 GPa, the changes of Y_l, Y_l' will be within the experimental error. This stress hardening was macroscopically observable in the PPTA single fiber. As mentioned before, if the stress hardening is mainly due to the elongation of the molecular chains after the micro-fibril orientation along the fiber axis, the crystallite orientation of PPTA fiber was considered to change simultaneously with the macroscopic stress hardening.

Figure 5 shows the stress dependence of the F_w value for the 200 reflection of the PPTA single fiber along the azimuthal angle. All plots were perfectly reversible after unloading. The F_w value decreased abruptly at the initial stage of the tensile stress, which indicates that the degree of the crystallite orientation was getting higher. These results suggest that the crystallite orientation may partly contribute to increasing the steepness of the slope of the macroscopic stress–strain curve. However, an inflection point, which was almost half of that (1100 MPa) appearing in the macroscopic stress–strain curve, was observed at around 600 MPa of tensile stress in the F_w value–stress curve. This indicated that the change of the micro-fibril orientation alone was insufficient to explain the macroscopic stress hardening, and an alternative mechanism had to be considered. Next, we focused on the mechanical properties of the crystalline regions for the PPTA fiber along the fiber axis using synchrotron X-ray diffraction.

Figure 6 shows the 006 diffraction profiles before loading and under loading of 1390 MPa and 2270 MPa. The diffraction peak shifted to a lower angle when the tensile stress was applied. This means the crystal lattice was extended along the chain axis by the tensile stress. The extensions of the crystal lattice were perfectly reversible.

Figure 7 shows the stress–strain curve for the (006) plane of PPTA at room temperature. The filled circles are the results for the single fiber measured using
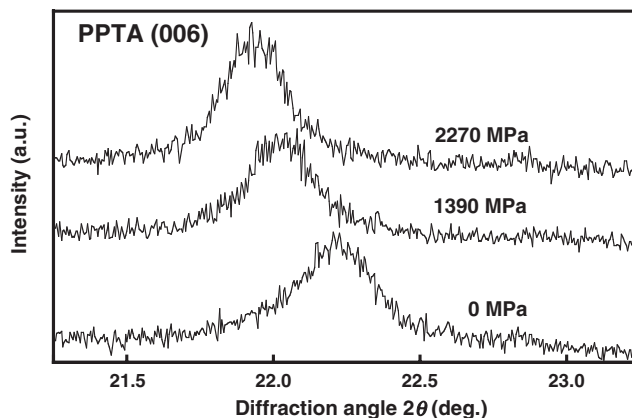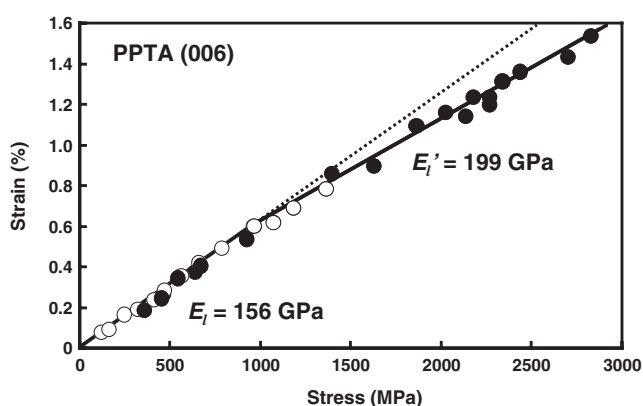

Figure 7. Stress-strain curve for the (006) plane of PPTA in the direction parallel to the chain axis. (○): previous results for fiber bundle using conventional X-ray generator, (●): single fiber using SPring-8 in this study.

SPring-8 synchrotron radiation, and the open circles are those reported for the fiber bundle using conventional X-ray generator equipment.[12–14] The results for the single fiber coincided with those for the fiber bundle, however, the stress applied to the fiber bundle was restricted to less than 1500 MPa. In contrast, macroscopic stress could be applied to a single fiber up to 2800 MPa (corresponding to a tensile load of 33 g), which is almost equal to the tensile strength of the fiber. The conventional method using the fiber bundle has not been able to reach this stress level. This shows that the SPring-8 synchrotron radiation is a powerful tool for researching the deformation behavior of polymer single fibers. With increasing the tensile stress, the crystal strain increased almost linearly in the initial stage of tensile stress (<1000 MPa). The initial inclination of the stress–strain curve gave an E_l value of 156 GPa, which coincided exactly with the value previously reported using the fiber bundle.[12–14] These results confirmed that the stress inhomogeneity within the fiber bundle could be negligibly small. As with macroscopic tensile behavior, stress hardening

was observed for the crystalline region of PPTA. From the stress–strain curve of the crystal lattice in Figure 7, the inclination of the curve changed around tensile stress of 1000 MPa. This indicates that the deformation mechanism of the crystal lattice in the higher tensile stress regions ($>$1000 MPa) was different from that in the initial stage. The inclination of the stress–strain curve in the higher stress region gave the E_l' value of 199 GPa. As shown in Figure 4, the inflection point in the macroscopic tensile behavior was observed at around 1100 MPa, the same point as in the PPTA crystal lattice. It is concluded that the stress hardening in the PPTA crystalline regions directly influenced the stress hardening of the macroscopic single fiber. Accordingly, the stress hardening of macroscopic PPTA fiber was affected not by the change of the fibril orientation along the fiber axis as reported by Northolt *et al.*, but by the change of the deformation mechanism of the molecular chain in the PPTA crystalline region. In conclusion, high brilliant synchrotron radiation X-ray beam is a powerful tool to detect the crystalline regions during the tensile deformation of a polymer single fiber.

CONCLUSIONS

The elastic modulus E_l of the crystalline regions of PPTA single fiber in the direction parallel to the chain axis was measured by X-ray diffraction using SPring-8 synchrotron radiation. The E_l value of PPTA single fiber was obtained as 156 GPa in the initial stage of tensile deformation. This value coincided with that previously reported for the fiber bundle. In addition, the inclination of the stress–strain curve in the PPTA crystalline regions changed at a tensile stress of around 1000 MPa. Stress hardening in the PPTA crystalline regions was observed during the tensile deformation process. The E_l' value was obtained as 199 GPa at the higher stress regions. This stress hardening was also observed at the same stress as macroscopic tensile deformation. These indicate that the deformation mechanism in the crystal lattice directly affected the macroscopic tensile deformation.

REFERENCES

1. L. A. Pilato and M. J. Michino, in "Advanced Composite Materials," Springer-Verlag, Berlin, 1994.

2. H. H. Yang, in "Kevlar Aramid Fiber," John Wiley & Sons, New York, 1993.

3. W. B. Black, *J. Macromol. Sci.*, **A7**, 3 (1973).

4. M. G. Dobb, D. J. Johnson, and B. P. Saville, *J. Polym. Sci., Polym. Phys. Ed.*, **15**, 2201 (1977).

5. S. Manabe, S. Kajita, and K. Kamide, *Sen'i Kikai Gakkaishi*, **33**, T93 (1980).

6. M. Panar, P. Avakian, R. C. Blume, K. H. Gardner, T. D. Gierke, and H. H. Yang, *J. Polym. Sci., Polym. Phys. Ed.*, **21**, 1955 (1983).

7. M. G. Northolt and J. J. van Aartsen, *J. Polym. Sci., Polym. Symp.*, **58**, 283 (1973).

8. M. G. Northolt, *Polymer*, **21**, 1199 (1980).

9. K. Prasad and D. T. Grubb, *J. Appl. Polym. Sci.*, **41**, 2189 (1990).

10. R. J. Young, D. Lu, R. J. Day, W. F. Knoff, and H. A. Davis, *J. Mater. Sci.*, **27**, 5431 (1992).

11. W.-Y. Yeh and R. J. Young, *Polymer*, **40**, 857 (1999).

12. K. Nakamae, T. Nishino, Y. Shimizu, K. Hata, and T. Matsumoto, *Kobunshi Ronbunshu*, **43**, 499 (1986).

13. K. Nakamae, T. Nishino, Y. Shimizu, and T. Matsumoto, *Kobunshi Ronbunshu*, **45**, 573 (1988).

14. K. Nakamae, T. Nishino, Y. Shimizu, and T. Matsumoto, *Polym. J.*, **19**, 451 (1987).

15. K. Nakamae, T. Nishino, and X. Airu, *Polymer*, **33**, 4898 (1992).

16. T. Ii, K. Tashiro, M. Kobayashi, and H. Tadokoro, *Macromolecules*, **20**, 347 (1987).

17. C. Riekel, T. Dieing, P. Engström, L. Vincze, C. Martin, and A. Mahendrasingam, *Macromolecules*, **32**, 7859 (1999).

18. Y. Li, C. Wu, and B. Chu, *J. Polym. Sci., Part B: Polym. Phys.*, **29**, 1309 (1991).

19. B. Chu, C. Wu, Y. Li, G. S. Harbison, E. J. Roche, S. R. Allen, T. F. Mcnulty, and J. C. Phillips, *J. Polym. Sci., Polym. Lett.*, **28**, 227 (1990).

20. S. Ran, D. Fang, X. Zong, B. S. Hsiao, B. Chu, and P. M. Cunniff, *Polymer*, **42**, 1601 (2001).

21. R. J. Gaymans, J. Tijssen, S. Harkema, and A. Bantjes, *Polymer*, **17**, 517 (1976).

22. R. J. Davies, M. Burghammer, and C. Riekel, *Macromolecules*, **39**, 4834 (2006).

23. I. Sakurada, T. Ito, and K. Nakamae, *Makromol. Chem.*, **75**, 1 (1964).

24. K. Nakamae and T. Nishino, in "Integration of Fundamental Polymer Science and Technology-5," Elsevier, New York, 121, 1991.

25. K. Nakamae and T. Nishino, *Adv. X-ray Anal.*, **35**, 545 (1992).

26. T. Nishino, M. Kotera, K. Okada, H. Sakurai, K. Nakamae, Y. Katsuya, Y. Kagoshima, Y. Tsusaka, and J. Matsui, *Mater. Sci. Res. Int., Special Technical Publication–1*, 378 (2001).

27. M. G. Northolt and J. J. van Aartsen, *J. Polym. Sci., Polym. Lett. Ed.*, **11**, 337 (1973).

28. A. M. Hindeleh, N. A. Halim, and K. A. Ziq, *J. Macromol. Sci., Phys.*, **B23**, 289 (1984).

29. K. Kaji, *Report of Poval Committee*, **66**, 113 (1975).